

Neural Collapse-Inspired Multi-Label Federated Learning under Label-Distribution Skew

Can Peng¹, Yuyuan Liu¹, Yingyu Yang¹, Prमित Saha¹, Qianye Yang¹, J. Alison Noble¹

¹University of Oxford, Oxford, United Kingdom

Abstract

Federated Learning (FL) enables collaborative model training across distributed clients while preserving data privacy. However, the performance of deep learning often deteriorates in FL due to decentralized and heterogeneous data. This challenge is further amplified in multi-label scenarios, where data exhibit complex characteristics such as label co-occurrence, inter-label dependency, and discrepancies between local and global label relationships. While most existing FL research primarily focuses on single-label classification, many real-world applications, particularly in domains such as medical imaging, often involve multi-label settings. In this paper, we address this important yet underexplored scenario in FL, where clients hold multi-label data with skewed label distributions. Neural Collapse (NC) describes a geometric structure in the latent feature space where features of each class collapse to their class mean with vanishing intra-class variance, and the class means form a maximally separated configuration. Motivated by this theory, we propose a method to align feature distributions across clients and to learn high-quality, well-clustered representations. To make the NC-structure applicable to multi-label settings, where image-level features may contain multiple semantic concepts, we introduce a feature disentanglement module that extracts semantically specific features. The clustering of these disentangled class-wise features is guided by a predefined shared NC structure, which mitigates potential conflicts between client models due to diverse local data distributions. In addition, we design regularisation losses to encourage compact clustering in the latent feature space. Experiments conducted on four benchmark datasets across eight diverse settings demonstrate that our approach outperforms existing methods, validating its effectiveness in this challenging FL scenario.

Introduction

Federated Learning (FL) has emerged as a promising framework for analysing sensitive data, particularly in domains like healthcare imaging, where privacy and legal constraints prevent direct data sharing. However, most existing FL approaches are limited to basic multi-class classification tasks, failing to account for more realistic scenarios where multiple labels frequently co-occur within a single sample. For

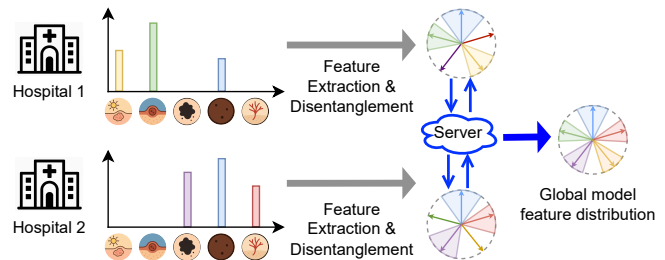


Figure 1: Within an FL system, clients may present distinct data distributions and label relationships. For example, Client 1 primarily serves patients with sun exposure-related skin lesions, whereas Client 2 mainly handles cases involving melanoma and vascular lesions. The proposed method aims to address multi-label, label-skewed FL scenarios by disentangling class-specific features and promoting structured feature clustering in the latent feature space.

instance, many diseases are interrelated, and patients often present with multiple conditions or symptoms simultaneously, rather than a single isolated issue. This multi-label nature of real-world data is often overlooked. Another core challenge in FL is data heterogeneity across clients, as each client (e.g., hospital) may possess a uniquely skewed data distribution. This variation arises from differences in geography, population demographics, medical facilities, and clinical expertise. As a result, clients may exhibit label imbalance, including majority, minority, or even missing (vacant) classes. Under multi-label scenarios, such heterogeneity becomes even more pronounced, making collaboration across clients significantly more difficult. Figure 1 illustrates this scenario, demonstrating that hospitals may hold datasets containing various sets of dermatological conditions.

In this paper, we explore the problem of multi-label FL under label-skewed conditions, where each client’s local data is both imbalanced and divergent from the global distribution. Without directly sharing local data, the goal is to collaboratively train a global model that performs well across all target classes, despite the presence of class imbalance and missing labels on certain clients. To tackle the unique challenges posed by multi-label, label-skewed FL, we propose a novel method called Federated Neural Collapse Alignment for Multi-Label

Learning (FedNCAlign-ML). Our approach introduces a representation learning framework for multi-label FL, inspired by Neural Collapse (NC) theory (Papayan et al., 2020), to enhance feature alignment across clients with heterogeneous label distributions. Specifically, we first encode each input image using a standard feature extractor, producing an image-level representation potentially containing multiple semantic concepts. We then leverage attention mechanisms to extract class-specific representations from this image-level representation, generating disentangled, class-wise embeddings. This effectively decomposes the complex multi-label problem into multiple single-label problems. Next, motivated by the NC phenomenon, we incorporate a predefined Equiangular Tight Frame (ETF) structure to promote consistent and discriminative feature alignment across clients, even under non-IID data distributions. The ETF structure facilitates class-independent clustering, encouraging local models to align with the global class geometry rather than overfitting to their local data distributions. Additionally, we introduce two complementary regularisation terms to enhance feature clustering in the latent feature space. A rejection loss filters out noisy signals from negative features, and a contrastive loss encourages compact intra-class clustering and clear inter-class separation. The key contributions of this paper are as follows:

- We explore the important yet underexplored problem of multi-label FL under label-skewed conditions. To this end, we propose FedNCAlign-ML, a novel method inspired by Neural Collapse theory.
- FedNCAlign-ML effectively adapts established representation learning techniques from the multi-class to the multi-label setting, and tackles the challenges introduced by heterogeneous local data distributions, label co-occurrence, and inter-label dependency.
- To handle the presence of multiple semantic concepts within multi-label samples, we introduce an attention-based feature disentanglement block that extracts class-specific representations from image-level features. Additionally, we incorporate two regularisation terms, one to suppress noisy negative features and another to promote compact class-wise clustering.
- We evaluate the proposed FedNCAlign-ML method on four benchmark datasets under eight diverse settings, comparing it to state-of-the-art FL approaches. The results show that FedNCAlign-ML consistently outperforms existing methods, achieving improvements of up to 2.87% in class-wise AUC and 7.29% in class-wise F1 score.

Related Work

Heterogeneous Federated Learning

The foundational FL algorithm, FedAvg (McMahan et al., 2017), performs iterative weighted averaging of locally trained model parameters. This process involves local training on

client devices, aggregation at a central server, and broadcasting the updated global model back to clients. While FedAvg performs well under independently and identically distributed (IID) data, real-world scenarios often involve non-IID data distributions. These distributions are commonly observed as quantity skew, label distribution skew, and feature distribution skew, all of which present significant challenges for FL. In the context of multi-class classification, numerous methods have been proposed to address such data heterogeneity within FL settings. For instance, FedProx (Li et al., 2020) adds an L2 regularisation term to constrain local updates and encourage proximity to the global model. FedCurv (Shoham et al., 2019) uses Elastic Weight Consolidation (Kirkpatrick et al., 2017) to preserve important local parameters to reduce divergence across clients. SCAFFOLD (Karimireddy et al., 2020) introduces control variates to correct client drift. SphereFed (Dong et al., 2022) projects features onto a hypersphere using a fixed classifier to mitigate latent feature distribution discrepancies. FedVLS (Guo et al., 2025) applies global model distillation to alleviate forgetting of missing classes and regularisation to amplify minority class losses, thereby improving performance on underrepresented classes. Although these approaches have demonstrated effectiveness in the multi-class setting, their performance tends to deteriorate when directly applied to the more complex multi-label scenario, where each sample may be associated with multiple co-occurring labels. In this work, we focus on addressing the challenges of multi-label FL under quantity-skewed and label-skewed data distribution.

Multi-Label Federated Learning

Although multi-label classification is a fundamental task, it remains less explored than multi-class classification in image processing. In the context of FL, the multi-label setting introduces additional and distinct challenges compared to the multi-class scenario, including label co-occurrence, inter-label dependency, and divergence between local and global label relationships. FedLGT (Liu et al., 2024) addresses these challenges by focusing on modelling label correlations across clients. Building upon C-Tran (Lanchantin et al., 2021), it leverages frozen CLIP (Radford et al., 2021) text embeddings to maintain consistent label relationships and reduce divergence in label dependencies among clients. In contrast, our approach focuses on understanding the structure of the latent feature space and explicitly controlling and optimising it to enhance robustness under challenging label-skewed FL conditions.

Neural Collapse-Inspired Methods

Recent research has shown that during the terminal phase of training (TPT), a phenomenon known as Neural Collapse (NC) emerges (Papayan et al., 2020). TPT refers to the stage when overparameterized deep networks are trained on balanced multi-class classification datasets, and the model’s performance plateaus while the training loss remains non-zero and continues to decrease. NC describes a distinctive geomet-

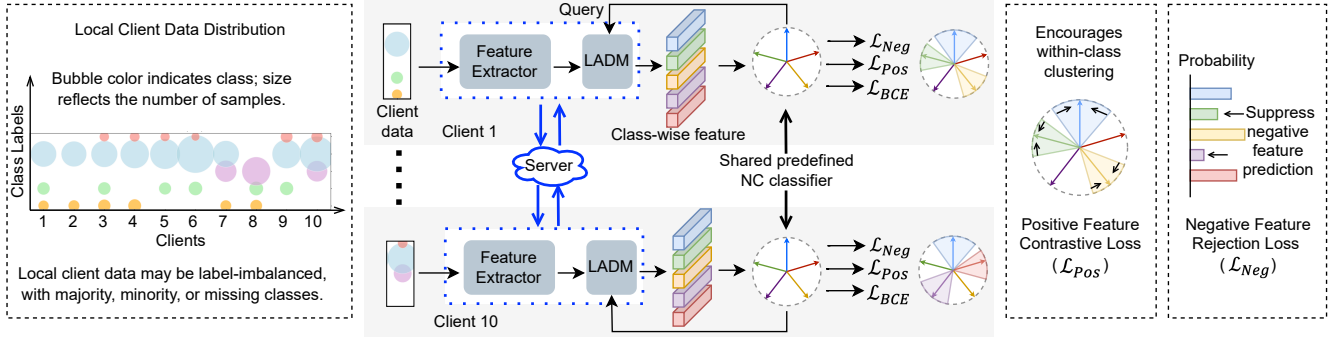


Figure 2: Framework for the proposed FedNCAAlign-ML method for addressing multi-label, label-skewed FL. First, an attention-based Label-Aware Disentanglement Module (LADM) extracts label-specific features from image-level representations. Then, a predefined ETF matrix serves as both the shared classifier and the source of class-wise query embeddings, enabling consistent local training across clients. Additionally, two regularisation terms are introduced to suppress noisy negative features and encourage compact intra-class clustering in the latent feature space.

ric structure in the latent feature space: final-layer features collapse to their corresponding within-class means, and these class-wise prototypes align to form the vertices of a simplex Equiangular Tight Frame (ETF). As this simple yet elegant mathematical structure provides an optimal linear separable state for classification, NC-inspired classifiers have been explored in various domains, including federated learning (Li et al., 2023b), incremental learning (Yang et al., 2023b; Wei et al., 2025), few-shot learning (Yang et al., 2023b), and long-tail recognition (Gao et al., 2024). Despite growing interest, most existing work has focused on multi-class classification, while the equally important challenge of multi-label classification remains underexplored. To address this gap, Li et al. (2023a) investigates the presence of NC in multi-label settings. They find that network training on a balanced multi-label dataset also exhibits NC but in a generalised form. In particular, features corresponding to single-label instances still conform to the Simplex ETF structure, while features associated with multi-label instances tend to approximate scaled averages of the single-label prototypes. MLC-NC (Tao et al., 2025) uses NC to process the long-tailed multi-label classification task in a centralised setting. However, it does not consider the missing class condition, which frequently arises in label-skewed FL scenarios across individual clients. To the best of our knowledge, our paper is the first to explore multi-label FL from an NC perspective. It opens the possibility to solve the heterogeneous multi-label FL challenge by fundamentally avoiding interference due to various local data distributions, label co-occurrence, and inter-label dependency.

Preliminaries

Problem Formulation

We consider a multi-label, label-skewed FL setting with K clients collaboratively training a shared global model. Each client k holds a private dataset $\mathcal{D}_k = \{(x_i^k, y_i^k)\}_{i=1}^{N_k}$ of size

N_k , where the input image $x_i^k \in \mathbb{R}^{H \times W \times 3}$ and the label $y_i^k \in \{0, 1\}^C$ is a multi-hot vector over the C classes. Let $\mathcal{C} = \{1, \dots, C\}$ denote the global class index set. Due to label skew, client k may only observe a subset $\mathcal{C}_k \subseteq \mathcal{C}$, and even for shared classes, the class-conditional distributions can differ across clients. The goal is to learn a single global model that accurately recognizes all classes in \mathcal{C} without sharing raw data among clients.

Neural Collapse (NC)

In this section, we first introduce the structure of the simplex ETF, followed by a discussion of the key properties of Neural Collapse.

Simplex Equiangular Tight Frame (ETF). A simplex ETF matrix $\mathbf{M} = [\mathbf{m}_c]_{c=1}^C \in \mathbb{R}^{d \times C}$ composed of C column vectors, each corresponding to a class prototype in $\mathbf{m}_c \in \mathbb{R}^d$. A standard construction is:

$$\mathbf{M} = \sqrt{\frac{C}{C-1}} \mathbf{U} \left(\mathbf{I}_C - \frac{1}{C} \mathbf{1}_C \mathbf{1}_C^\top \right), \quad (1)$$

where $\mathbf{U} \in \mathbb{R}^{d \times C}$ denotes a rotation orthogonal matrix ($\mathbf{U}^\top \mathbf{U} = \mathbf{I}_C$). \mathbf{I}_C is the $C \times C$ identity matrix. $\mathbf{1}_C$ is the C -dimensional all-ones vector.

This yields unit-norm columns with equal pairwise inner products:

$$\mathbf{m}_a^\top \mathbf{m}_b = \begin{cases} 1, & a = b, \\ -\frac{1}{C-1}, & a \neq b, \end{cases} \quad a, b \in \mathcal{C}. \quad (2)$$

Hence, all prototypes have equal ℓ_2 norm and identical pairwise angles, forming a centered regular simplex.

Neural Collapse properties. At the end of training, over-parameterized networks exhibit the NC phenomenon. Empirically, the following regularities are observed:

- **Variability Collapse** (\mathcal{NC}_1). Within-class feature variance collapses: features of the same class concentrate at their class mean.
- **Convergence to Simplex ETF** (\mathcal{NC}_2). Class means arrange as the vertices of a simplex ETF, forming a maximally symmetric and equidistant configuration.
- **Self-Duality** (\mathcal{NC}_3). Upon appropriate rescaling, the final-layer classifier weights align with the class means, sharing the same simplex ETF geometry.

Proposed Method

The NC phenomenon suggests a promising structure for optimal feature clustering in the latent feature space under well-trained conditions. We leverage this geometry to shape the latent feature space in the challenging multi-label FL setting, where client data often deviates from the global distribution. An overview of our framework is shown in Figure 2.

Label-Aware Disentanglement Module (LADM)

Multi-label images may contain multiple object categories, making a single pooled representation suboptimal because it compresses multiple semantics into one vector. Inspired by recent advances in multi-label learning (Liu et al., 2021; Ridnik et al., 2023; Xu et al., 2023), we incorporate an attention mechanism to extract class-specific information from the image-level representation, thereby enhancing the discriminative power of each label.

For client k , each sample $x_i^k \in \mathcal{D}_k$ ($i \in [N_k]$) is processed by a backbone to produce an image-level feature $\mathbf{f}_i^k \in \mathbb{R}^d$. For notational convenience, we drop the client index and write \mathbf{f}_i for \mathbf{f}_i^k in what follows. The feature \mathbf{f}_i is then passed to the Label-Aware Disentanglement Module (LADM), which utilises a 4-head cross-attention mechanism to derive label-specific features. In the FL setting, each client trains exclusively on its local data, which often deviates significantly across clients and from the global distribution. To ensure a consistent feature extraction strategy across clients, we adopt a predefined simplex ETF matrix, $\mathbf{M} = [\mathbf{m}_c]_{c=1}^C \in \mathbb{R}^{d \times C}$. Its columns serve both as fixed classifier weights and as class-wise queries for LADM. LADM applies cross-attention from each query \mathbf{m}_c to the image feature \mathbf{f}_i to obtain the class-wise feature:

$$\mathbf{h}_{ic} = \text{MultiHeadAttn}(\mathbf{m}_c, \mathbf{f}_i), \quad c \in \mathcal{C} \quad (3)$$

and stacks them into

$$\mathbf{H}_i = \begin{bmatrix} \mathbf{h}_{i1}^\top \\ \vdots \\ \mathbf{h}_{iC}^\top \end{bmatrix} \in \mathbb{R}^{C \times d}. \quad (4)$$

Sharing the fixed query matrix \mathbf{M} across clients mitigates aggregation conflicts and encourages globally aligned, disentangled features.

Neural Collapse-Inspired Feature Alignment

After disentangling image-level features into class-wise representations with LADM, each sample $i \in [N_k]$ yields a feature $\mathbf{h}_{ic} \in \mathbb{R}^d$ for every class $c \in \mathcal{C}$. To avoid client-specific classifier drift caused by label imbalance or missing classes, we fix the classifier to the global simplex ETF used as the LADM query matrix, $\mathbf{M} = [\mathbf{m}_c]_{c=1}^C \in \mathbb{R}^{d \times C}$. Given \mathbf{h}_{ic} and its corresponding prototype \mathbf{m}_c , we compute a class logit and pass it through the sigmoid to obtain a binary prediction:

$$\hat{y}_{ic} = \sigma(\mathbf{h}_{ic}^\top \mathbf{m}_c), \quad (5)$$

and train with a binary cross-entropy (BCE) objective

$$\mathcal{L}_{\text{BCE}} = -\frac{1}{N} \frac{1}{C} \sum_{i=1}^N \sum_{c=1}^C \left[y_{ic} \log \hat{y}_{ic} + (1 - y_{ic}) \log(1 - \hat{y}_{ic}) \right]. \quad (6)$$

Here, $y_{ic} \in \{0, 1\}$ is the ground-truth multi-label indicator, $\sigma(\cdot)$ denotes the sigmoid. This fixed classifier improves class separability and reduces divergence between local and global label distributions.

Reducing Noise and Improving Clustering

Each sample produces C class-wise features $\{\mathbf{h}_{ic}\}_{c=1}^C$. Let the positive and negative class sets for sample i be $\mathcal{C}_i^+ = \{c \mid y_{ic} = 1\}$ and $\mathcal{C}_i^- = \{c \mid y_{ic} = 0\}$, respectively. We introduce two regularizers: one to suppress noise from negative features and another to encourage compact clustering of positive features.

Negative Feature Rejection Loss. While \mathcal{L}_{BCE} discourages alignment of a negative feature \mathbf{h}_{ic} with its own prototype \mathbf{m}_c when $y_{ic} = 0$, it does not prevent \mathbf{h}_{ic} from spuriously aligning with other prototypes. We therefore penalize high similarity between every negative feature and all non-self prototypes:

$$\hat{s}_{icr} = \sigma(\mathbf{h}_{ic}^\top \mathbf{m}_r), \quad c \in \mathcal{C}_i^-, r \in \mathcal{C} \setminus \{c\}, \quad (7)$$

$$\mathcal{L}_{\text{Neg}} = -\frac{1}{N} \sum_{i=1}^N \frac{1}{|\mathcal{C}_i^-|} \sum_{c \in \mathcal{C}_i^-} \frac{1}{C-1} \sum_{\substack{r=1 \\ r \neq c}}^C \mathbb{I}(\hat{s}_{icr} > \tau) \log(1 - \hat{s}_{icr}). \quad (8)$$

The indicator $\mathbb{I}(\cdot)$ filters out low-similarity pairs so that only confident negatives contribute. In our experiments, we set $\tau = 0.3$.

Positive Feature Contrastive Loss. To encourage compact and discriminative class-wise clustering in the latent feature space, we introduce a contrastive loss. This loss enforces each positive feature \mathbf{h}_{ic} to be closer to its own prototype than to others via a prototype-softmax:

$$\mathcal{L}_{\text{Pos}} = -\frac{1}{N} \sum_{i=1}^N \frac{1}{|\mathcal{C}_i^+|} \sum_{c \in \mathcal{C}_i^+} \log \frac{\exp(\mathbf{h}_{ic}^\top \mathbf{m}_c)}{\sum_{r=1}^C \exp(\mathbf{h}_{ic}^\top \mathbf{m}_r)}. \quad (9)$$

Total Objective. The total loss can be expressed as:

$$\mathcal{L}_{\text{total}} = \mathcal{L}_{\text{BCE}} + \lambda_1 \mathcal{L}_{\text{Neg}} + \lambda_2 \mathcal{L}_{\text{Pos}}. \quad (10)$$

where $\lambda_1, \lambda_2 \geq 0$ balance the contributions of the regularizers.

FedNCAAlign-ML

We propose FedNCAAlign-ML, a framework that enhances the standard FL protocol with an NC-inspired local training strategy tailored for multi-label tasks and skewed local data distributions. In this framework, each client first encodes its input images into features, which are then disentangled into class-specific embeddings using LADM. These embeddings are aligned with a shared simplex ETF matrix that serves simultaneously as fixed classifier prototypes and as class-wise queries for LADM, thereby enforcing a consistent global geometry across clients despite label imbalance. To further improve representation quality, we incorporate two regularizers: (i) a negative rejection loss to suppress spurious alignments of irrelevant features, and (ii) a positive contrastive loss to encourage compact intra-class clustering and clear inter-class separation. The novelty of FedNCAAlign-ML lies in this local training design, which integrates disentangled class-wise embeddings, ETF-based alignment, and geometry-aware regularization. The complete procedure is summarized in Algorithm 1.

Algorithm 1: FedNCAAlign-ML: Federated Neural Collapse Alignment for Multi-Label Learning

Input: K clients with datasets $\{\mathcal{D}_k\}_{k=1}^K$; initial global model w_0 ; predefined ETF matrix \mathbf{M} ; learning rate η ; local epochs E ; communication rounds T .

```

1: Server executes:
2: Initialize  $w \leftarrow w_0$ 
3: for  $t = 0$  to  $T - 1$  do ▷ communication rounds
4:   for each client  $k \in \{1, \dots, K\}$  in parallel do
5:      $w_{t+1}^k \leftarrow \text{CLIENTUPDATE}(\mathcal{D}_k, w_t, \mathbf{M})$ 
6:   end for
7:    $w_{t+1} \leftarrow \text{MODELAGGREGATION}(\{w_{t+1}^k\}_{k=1}^K)$ 
8:   Broadcast  $w_{t+1}$  to all clients
9: end for

10: function CLIENTUPDATE( $\mathcal{D}_k, w, \mathbf{M}$ )
11:   for  $e = 1$  to  $E$  do ▷ local epochs
12:     for each batch  $(x, y) \subset \mathcal{D}_k$  do
13:        $\mathbf{f} \leftarrow \text{FEATUREEXTRACTOR}(w, x)$ 
14:        $\mathbf{H} \leftarrow \text{LADM}(\mathbf{f}, \mathbf{M})$ 
15:       Compute prediction  $\hat{y}_c = \sigma(\mathbf{h}_c^\top \mathbf{m}_c)$  ▷ Eqs. 5
16:       Compute loss  $\mathcal{L}_{\text{total}}(w; \mathbf{M}, \mathbf{H}, \hat{\mathbf{y}})$  ▷ Eqs. 6, 8, 9, 10
17:       Update  $w \leftarrow w - \eta \nabla_w \mathcal{L}_{\text{total}}$ 
18:     end for
19:   end for
20:   return  $w$ 
21: end function

```

Experiment

Dataset and Evaluation Metric

Datasets: We conduct experiments on both general computer vision (CV) datasets and medical imaging datasets to evaluate

the effectiveness and real-world applicability of the proposed method. For general CV tasks, we use CIFAR-10 (Krizhevsky et al., 2009) and PASCAL VOC (Everingham et al., 2010). Since CIFAR-10 is originally a multi-class dataset, we adopt the method used by Li et al. (2023a) to transform it into a multi-label dataset. This is done by merging multiple images into a single composite image, with the combined labels serving as the new ground truth. For medical imaging tasks, we use DermaMNIST (Yang et al., 2023a) and ChestX-ray14 (Wang et al., 2017). DermaMNIST, which originally contains 7 skin disease categories in a multi-class format, is converted to a multi-label dataset using the same strategy applied to CIFAR-10. ChestX-ray14 is naturally a multi-label dataset, comprising 14 thoracic disease categories and an additional ‘‘No Finding’’ label. Since a significant portion of the dataset, approximately four-sevenths of the training data, are ‘‘No Finding’’ samples (negative cases with all-zero labels), we distribute these samples evenly across all clients. This setup mimics a realistic clinical scenario in which healthy cases are prevalent, while disease cases are relatively rare and unevenly distributed across clients. Detailed information about the datasets and local data distributions under various experimental settings is provided in the Appendix.

Evaluation Metric: Given our focus on label-skewed data distributions, where certain classes may be missing or underrepresented, we report both overall (micro) and class-wise (macro) performance metrics. Following standard practices across different datasets, we report AUC and F1 scores for CIFAR-10, PASCAL VOC, and DermaMNIST, and AUC for ChestX-ray14. Together, these metrics offer a balanced and comprehensive evaluation by capturing both overall performance and class-specific behaviour.

Task Setup and Implementation Details

Task Setup: We simulate the FL system with 10 clients and adopt a full client participation strategy. To reflect the standard heterogeneous FL setting, we introduce non-IID data distributions by partitioning the data using a Dirichlet distribution, parameterised by the concentration factor β . To further emulate label-skewed scenarios, we define a class presence ratio γ , which limits the number of classes available to each client and simulates cases where certain classes are entirely absent from local datasets.

Implementation Details: For all experiments, we use ResNet-18 (He et al., 2016) as the feature extractor. Each FL global model is trained over 100 communication rounds, with one epoch of local training per round. The final model is selected based on its best performance on the validation set. We use a batch size of 32 and initialise the learning rate at 1×10^{-4} , using the AdamW optimiser with a weight decay of 0.01. Models for the CIFAR-10 dataset are trained from scratch, while models for other datasets are initialised with ImageNet-pretrained weights. During training, the regularisation hyperparameter λ_1 is empirically set to either 1 or 0.01, depending on the background complexity of the dataset. For datasets with complex backgrounds, where disentangling class-specific features

| | $\beta = 0.5, \gamma = 0.5$ | | | | $\beta = 0.1, \gamma = 0.5$ | | | |
|-------------------------------------|-----------------------------|--------------|--------------|--------------|-----------------------------|--------------|--------------|--------------|
| | macro-AUC | macro-F1 | AUC | F1 | macro-AUC | macro-F1 | AUC | F1 |
| Centralized (Upperbound) | 91.17 | 61.40 | 91.04 | 62.22 | 91.17 | 61.40 | 91.04 | 62.22 |
| FedAvg (McMahan et al., 2017) | 82.46 | 40.65 | 81.83 | 41.24 | 78.84 | 31.15 | 77.00 | 34.98 |
| FedCurv (Shoham et al., 2019) | 82.19 | 39.36 | 81.81 | 39.61 | 79.03 | 32.31 | 77.97 | 36.13 |
| FedProx (Li et al., 2020) | 82.23 | 39.37 | 81.68 | 39.27 | 79.40 | 31.01 | 76.69 | 35.73 |
| SCAFFOLD (Karimireddy et al., 2020) | 82.01 | 38.41 | 81.49 | 38.83 | 79.29 | 32.38 | 77.74 | 35.90 |
| SphereFed (Dong et al., 2022) | 84.85 | 47.58 | 85.04 | 47.29 | 83.27 | 39.52 | 79.45 | 40.77 |
| FedLGT (Liu et al., 2024) | 84.24 | 45.45 | 84.16 | 45.99 | 81.44 | 35.95 | 81.49 | 38.78 |
| FedNCAIalign-ML (ours) | 87.72 | 49.22 | 87.13 | 49.60 | 84.07 | <u>38.14</u> | <u>79.56</u> | 42.85 |

Table 1: Comparisons on the multi-label CIFAR-10 dataset (Krizhevsky et al., 2009). Non-IID data distributions across clients are simulated using the Dirichlet concentration parameter (β) and the class-missing ratio (γ).

| | $\beta = 0.5, \gamma = 0.71$ | | | | $\beta = 0.1, \gamma = 0.71$ | | | |
|-------------------------------------|------------------------------|--------------|--------------|--------------|------------------------------|--------------|--------------|--------------|
| | macro-AUC | macro-F1 | AUC | F1 | macro-AUC | macro-F1 | AUC | F1 |
| Centralized (Upperbound) | 91.86 | 63.49 | 94.52 | 73.30 | 91.86 | 63.49 | 94.52 | 73.30 |
| FedAvg (McMahan et al., 2017) | 90.18 | 53.96 | <u>92.68</u> | 67.53 | 83.95 | 40.69 | 86.68 | 63.03 |
| FedCurv (Shoham et al., 2019) | <u>90.31</u> | 56.17 | 92.64 | <u>68.11</u> | <u>86.20</u> | 42.19 | <u>89.54</u> | 64.76 |
| FedProx (Li et al., 2020) | 90.16 | 55.85 | 92.44 | 67.95 | 83.73 | 42.98 | 87.96 | 63.50 |
| SCAFFOLD (Karimireddy et al., 2020) | 89.56 | 54.88 | 92.13 | 67.59 | 85.33 | 43.60 | 89.41 | <u>64.75</u> |
| SphereFed (Dong et al., 2022) | 85.36 | 44.25 | 89.46 | 53.40 | 83.37 | 41.90 | 88.92 | 50.94 |
| FedLGT (Liu et al., 2024) | 87.33 | <u>56.24</u> | 90.84 | 68.25 | 84.80 | <u>44.09</u> | 88.70 | 57.35 |
| FedNCAIalign-ML (ours) | 90.42 | 56.39 | 92.95 | 67.78 | 87.69 | 51.38 | 90.36 | 63.26 |

Table 2: Comparisons on the multi-label DermaMNIST dataset (Yang et al., 2023a).

| | $\beta = 0.05, \gamma = 0.5$ | | | | $\beta = 0.01, \gamma = 0.5$ | | | |
|-------------------------------------|------------------------------|--------------|--------------|--------------|------------------------------|--------------|--------------|--------------|
| | macro-AUC | macro-F1 | AUC | F1 | macro-AUC | macro-F1 | AUC | F1 |
| Centralized (Upperbound) | 95.66 | 74.77 | 96.22 | 77.15 | 95.66 | 74.77 | 96.22 | 77.15 |
| FedAvg (McMahan et al., 2017) | 93.72 | 57.00 | 94.20 | 64.62 | 93.29 | 49.16 | 93.90 | 61.08 |
| FedCurv (Shoham et al., 2019) | <u>93.69</u> | 57.32 | 94.40 | 64.74 | <u>93.33</u> | 48.93 | 93.87 | 61.35 |
| FedProx (Li et al., 2020) | 93.70 | 57.08 | <u>94.26</u> | 64.46 | 93.05 | 48.99 | 93.74 | 61.16 |
| SCAFFOLD (Karimireddy et al., 2020) | 93.07 | 58.20 | 93.97 | 65.86 | 93.44 | 50.89 | <u>93.93</u> | 62.10 |
| SphereFed (Dong et al., 2022) | 85.72 | 33.71 | 87.38 | 38.19 | 86.85 | 32.44 | 87.94 | 36.18 |
| FedLGT (Liu et al., 2024) | 91.07 | <u>61.40</u> | 91.39 | <u>65.88</u> | 91.20 | <u>56.59</u> | 91.20 | <u>64.58</u> |
| FedNCAIalign-ML (ours) | 93.82 | 64.34 | 94.18 | 66.42 | 93.07 | 62.08 | 93.95 | 66.00 |

Table 3: Comparison of related FL methods with ours on the multi-label PASCAL VOC 2012 dataset (Everingham et al., 2010).

is more challenging, a smaller value ($\lambda_1 = 0.01$) is used to reduce potential interference with positive feature learning. The other regularisation hyperparameter, λ_2 , is fixed at 1 across all experiments.

Performance Comparison

To evaluate the effectiveness of the proposed method, we compare it with other methods across four datasets, as shown in Tables 1, 2, 3, and 4. As observed in these tables, our method consistently achieves the best performance in most cases across different datasets. The improvement is particularly notable on naturally long-tailed datasets such as DermaMNIST and ChestX-ray14, where our method yields substantial gains in class-wise performance, indicating its ability to produce more balanced predictions. Specifically, under the $\beta = 0.1$ setting on DermaMNIST, our method outperforms the second-best approach by 1.49% in class-wise AUC and 7.29% in class-wise F1 score. For PASCAL VOC, when each client is limited to a maximum of half the total classes, our method achieves im-

provements of 2.94% and 5.49% in class-wise F1 score under the $\beta = 0.05$ and $\beta = 0.01$ settings, respectively. For ChestX-ray14 under the $\beta = 0.5$ and $\beta = 0.1$ settings, our method improves class-wise AUC by 0.64% and 1.31%, respectively. Overall, across a range of non-IID configurations with limited class availability per client, our method consistently outperforms existing FL approaches, demonstrating strong robustness to various label-skewed data distributions.

Ablation Study

To evaluate the effectiveness of each component in the proposed method, we conducted an ablation study on the multi-label DermaMNIST dataset, with the client data distribution configured using $\beta = 0.1$ and $\gamma = 0.71$. The experimental results are presented in Table 5. As shown in the table, incorporating LADM for class-specific feature extraction, together with the predefined ETF classifier to encourage class-wise clustering alignment across clients in the latent feature space, yields improvements of 0.43% in class-wise AUC and

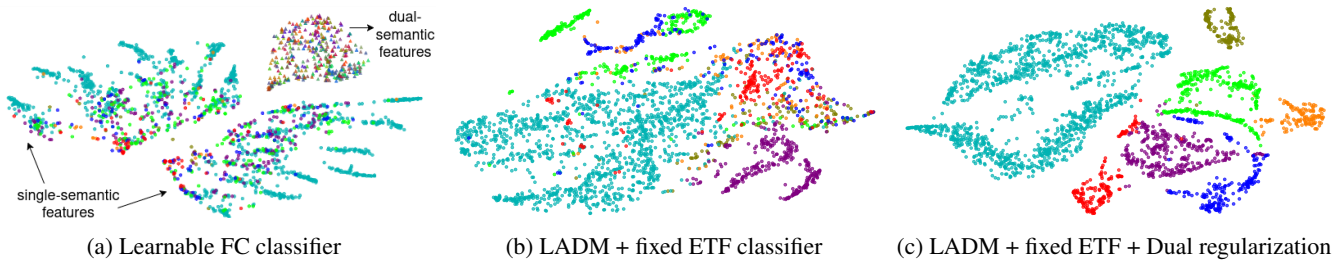


Figure 3: t-SNE visualisation of test data feature embeddings on the multi-label DermaMNIST experiment with $\beta = 0.1$, $\gamma = 0.71$. Each colour represents a class. Observing from subfigure (a), without feature disentanglement (LADM), the model relies on undesired information, such as the number of labels per sample, for clustering.

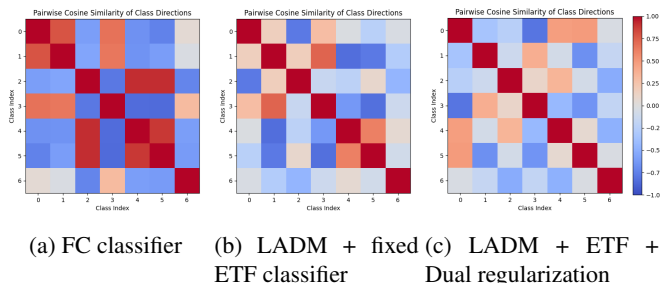


Figure 4: Pair-wise cosine similarity between test data class-wise average feature prototypes.

| | $\beta = 0.5, \gamma = 0.5$ | | $\beta = 0.1, \gamma = 0.5$ | |
|--------------|-----------------------------|--------------|-----------------------------|--------------|
| | macro-AUC | AUC | macro-AUC | AUC |
| Centralized | 71.44 | 79.62 | 71.44 | 79.62 |
| FedAvg | 69.07 | 73.28 | 69.84 | 78.00 |
| FedCurv | 68.12 | 72.15 | 69.46 | 77.63 |
| FedProx | 69.23 | 72.45 | 69.23 | 77.69 |
| SCAFFOLD | 69.02 | 72.21 | 66.71 | 78.69 |
| SphereFed | 57.48 | 70.26 | 61.80 | 74.59 |
| FedLGT | <u>69.76</u> | 72.41 | <u>70.02</u> | 77.93 |
| FedNAlign-ML | 70.40 | <u>72.62</u> | 71.33 | <u>78.10</u> |

Table 4: Comparison of related FL methods with ours on the ChestX-ray14 dataset (Wang et al., 2017).

7.34% in class-wise F1 score. Additional performance gains are achieved by introducing regularisation terms that enhance the model’s discriminative ability, resulting in further improvements of 3.31% in class-wise AUC and 3.43% in class-wise F1 score.

We also investigated the class-wise query mechanism within the attention-based LADM module. As reported in Table 6, fixed, well-designed class-wise queries consistently outperform learnable queries across most evaluation metrics. This outcome is intuitive in the context of label-skewed FL, where each client has a unique local data distribution. If the queries and classifier are learnable, the model may overfit to these local distributions, which can significantly deviate from the global distribution. Such overfitting introduces inconsistencies among client models and ultimately degrades the performance of the aggregated global model. To maintain consistent learn-

| ETF Clf | LADM | \mathcal{L}_{Neg} | \mathcal{L}_{Pos} | macro-AUC | macro-F1 | AUC | F1 |
|---------|------|---------------------|---------------------|--------------|--------------|--------------|--------------|
| | | | | 83.95 | 40.69 | 86.68 | 63.03 |
| ✓ | ✓ | | | 84.38 | 47.95 | 86.70 | 60.49 |
| ✓ | ✓ | ✓ | | 84.73 | 45.06 | 89.71 | 62.89 |
| ✓ | ✓ | | ✓ | 85.20 | 49.84 | 89.03 | 61.06 |
| ✓ | ✓ | ✓ | ✓ | 87.69 | 51.38 | 90.36 | 63.26 |

Table 5: Ablation study of the proposed method on the multi-label DermaMNIST dataset with $\beta = 0.1$, $\gamma = 0.71$.

| query type | query init | macro-AUC | macro-F1 | AUC | F1 |
|------------|------------|--------------|--------------|--------------|--------------|
| learnable | random | 82.94 | 47.94 | 86.33 | 57.37 |
| learnable | ETF | 85.39 | 46.92 | 84.94 | 53.37 |
| fixed | ETF | 84.38 | 47.95 | 86.70 | 60.49 |

Table 6: Ablation study of the class-wise feature extraction block - LADM on the multi-label DermaMNIST dataset.

ing across clients with non-iid data, it is therefore preferable to use predefined, well-separated, fixed embeddings to guide the learning process rather than relying on learnable representations.

To further analyse model behaviour, we present t-SNE visualisations of feature distributions from the test data in the latent feature space, generated under different model architectures and training strategies on the multi-label DermaMNIST dataset. The client data distribution is configured using $\beta = 0.1$ and $\gamma = 0.71$. As shown in Figure 3, when a conventional, learnable fully connected (FC) classifier is used, although the model achieves 83.95% class-wise AUC and 40.69% F1 score, the resulting feature representations exhibit poor clustering. Notably, the model appears to rely on undesired information. Specifically, it tends to group features based on the number of labels per sample, rather than focusing solely on semantic content. By incorporating LADM for extracting single-class features and employing a predefined ETF classifier to regulate feature distribution across clients, the model learns to focus more on semantic content for clustering. This leads to more disentangled, class-specific feature representations and improved clustering quality. Figure 4 also shows that the pairwise cosine similarity between class-wise average features is substantially reduced, indicating enhanced inter-class separability and stronger discriminative capability.

Finally, with the addition of extra regularisation terms during training, the feature clustering becomes more compact and semantically coherent, and the similarity among class-wise average prototypes is further reduced.

Conclusion

This paper investigates multi-label label-skewed FL, a practically important yet underexplored problem setting. This task is particularly challenging due to the complexities inherent in multi-label data, combined with difficulties introduced by the federated system, including heterogeneous local data distributions and inconsistencies between local and global data distributions. Inspired by Neural Collapse theory, we propose a feature disentanglement module and incorporate a predefined ETF structure to facilitate the extraction and clustering of class-specific representations, while also aligning feature distributions across clients in the latent feature space. Furthermore, we incorporate specific regularization losses to suppress noisy negative features and enhance compact class-wise clustering. Experiments on four benchmark datasets across eight settings show that our method outperforms existing approaches, with gains of up to 2.87% in class-wise AUC and 7.29% in class-wise F1 score.

Acknowledgments

This work was supported by the UKRI grant EP/X040186/1 (Turing AI Fellowship). This work was also partly supported by the InnoHK-funded Hong Kong Centre for Cerebrocardiovascular Health Engineering (COCHE) Project 2.1 (Cardiovascular risks in early life and fetal echocardiography).

References

Dong, X., Zhang, S. Q., Li, A., and Kung, H. (2022). Sphered: Hyperspherical federated learning. In *European Conference on Computer Vision*, pages 165–184. Springer.

Everingham, M., Van Gool, L., Williams, C. K., Winn, J., and Zisserman, A. (2010). The pascal visual object classes (voc) challenge. *International journal of computer vision*, 88:303–338.

Gao, J., Zhao, H., dan Guo, D., and Zha, H. (2024). Distribution alignment optimization through neural collapse for long-tailed classification. In *Forty-first International Conference on Machine Learning*.

Guo, K., Ding, Y., Liang, J., Wang, Z., He, R., and Tan, T. (2025). Exploring vacant classes in label-skewed federated learning. In *Proceedings of the AAAI Conference on Artificial Intelligence*, volume 39, pages 16960–16968.

He, K., Zhang, X., Ren, S., and Sun, J. (2016). Deep residual learning for image recognition. In *Proceedings of the IEEE conference on computer vision and pattern recognition*, pages 770–778.

Karimireddy, S. P., Kale, S., Mohri, M., Reddi, S., Stich, S., and Suresh, A. T. (2020). Scaffold: Stochastic controlled averaging for federated learning. In *International conference on machine learning*, pages 5132–5143. PMLR.

Kirkpatrick, J., Pascanu, R., Rabinowitz, N., Veness, J., Desjardins, G., Rusu, A. A., Milan, K., Quan, J., Ramalho, T., Grabska-Barwinska, A., et al. (2017). Overcoming catastrophic forgetting in neural networks. *Proceedings of the national academy of sciences*, 114(13):3521–3526.

Krizhevsky, A., Hinton, G., et al. (2009). Learning multiple layers of features from tiny images.

Lanchantin, J., Wang, T., Ordonez, V., and Qi, Y. (2021). General multi-label image classification with transformers. In *Proceedings of the IEEE/CVF conference on computer vision and pattern recognition*, pages 16478–16488.

Li, P., Wang, Y., Li, X., and Qu, Q. (2023a). Neural collapse in multi-label learning with pick-all-label loss.

Li, T., Sahu, A. K., Zaheer, M., Sanjabi, M., Talwalkar, A., and Smith, V. (2020). Federated optimization in heterogeneous networks. *Proceedings of Machine learning and systems*, 2:429–450.

Li, Z., Shang, X., He, R., Lin, T., and Wu, C. (2023b). No fear of classifier biases: Neural collapse inspired federated learning with synthetic and fixed classifier. In *Proceedings of the IEEE/CVF International Conference on Computer Vision*, pages 5319–5329.

Liu, I.-J., Lin, C.-S., Yang, F.-E., and Wang, Y.-C. F. (2024). Language-guided transformer for federated multi-label classification. In *Proceedings of the AAAI Conference on Artificial Intelligence*, volume 38, pages 13882–13890.

Liu, S., Zhang, L., Yang, X., Su, H., and Zhu, J. (2021). Query2label: A simple transformer way to multi-label classification. *arXiv preprint arXiv:2107.10834*.

McMahan, B., Moore, E., Ramage, D., Hampson, S., and y Arcas, B. A. (2017). Communication-efficient learning of deep networks from decentralized data. In *Artificial intelligence and statistics*, pages 1273–1282. PMLR.

Papayan, V., Han, X., and Donoho, D. L. (2020). Prevalence of neural collapse during the terminal phase of deep learning training. *Proceedings of the National Academy of Sciences*, 117(40):24652–24663.

Radford, A., Kim, J. W., Hallacy, C., Ramesh, A., Goh, G., Agarwal, S., Sastry, G., Askell, A., Mishkin, P., Clark, J., et al. (2021). Learning transferable visual models from natural language supervision. In *International conference on machine learning*, pages 8748–8763. PmLR.

- Ridnik, T., Sharir, G., Ben-Cohen, A., Ben-Baruch, E., and Noy, A. (2023). MI-decoder: Scalable and versatile classification head. In *Proceedings of the IEEE/CVF winter conference on applications of computer vision*, pages 32–41.
- Shoham, N., Avidor, T., Keren, A., Israel, N., Benditkis, D., Mor-Yosef, L., and Zeitak, I. (2019). Overcoming forgetting in federated learning on non-iid data. *arXiv preprint arXiv:1910.07796*.
- Tao, Z., Li, S.-Y., Wan, W., Zheng, J., Chen, J.-Y., Li, Y., Huang, S.-J., and Chen, S. (2025). Mlc-nc: Long-tailed multi-label image classification through the lens of neural collapse. In *Proceedings of the AAAI Conference on Artificial Intelligence*, volume 39, pages 20850–20858.
- Wang, X., Peng, Y., Lu, L., Lu, Z., Bagheri, M., and Summers, R. M. (2017). Chestx-ray8: Hospital-scale chest x-ray database and benchmarks on weakly-supervised classification and localization of common thorax diseases. In *Proceedings of the IEEE Conference on Computer Vision and Pattern Recognition (CVPR)*, pages 3462–3471.
- Wei, K., Xu, Z., and Deng, C. (2025). Compress to one point: Neural collapse for pre-trained model-based class-incremental learning. In *Proceedings of the AAAI Conference on Artificial Intelligence*, volume 39, pages 21465–21473.
- Xu, P., Xiao, L., Liu, B., Lu, S., Jing, L., and Yu, J. (2023). Label-specific feature augmentation for long-tailed multi-label text classification. In *Proceedings of the AAAI conference on artificial intelligence*, volume 37, pages 10602–10610.
- Yang, J., Shi, R., Wei, D., Liu, Z., Zhao, L., Ke, B., Pfister, H., and Ni, B. (2023a). Medmnist v2-a large-scale lightweight benchmark for 2d and 3d biomedical image classification. *Scientific Data*, 10(1):41.
- Yang, Y., Yuan, H., Li, X., Lin, Z., Torr, P., and Tao, D. (2023b). Neural collapse inspired feature-classifier alignment for few-shot class incremental learning. *arXiv preprint arXiv:2302.03004*.

Appendix

Ablation Study (additional)

To complement the results reported in the main manuscript, we present an additional ablation study to evaluate the contribution of each component in our proposed method. The experiments are conducted on the multi-label CIFAR-10 dataset (Krizhevsky et al., 2009), with the client data distribution configured using a Dirichlet concentration parameter $\beta = 0.5$ and a class-presenting ratio $\gamma = 0.5$. The experimental results are summarized in Tables 7 and 8, and Figures 5 and 6. As shown in Table 7, integrating LADM for class-specific feature extraction, along with the use of a predefined ETF classifier to encourage class-wise clustering alignment across clients in the latent feature space, leads to performance improvements of 3.38% in class-wise AUC and 3.99% in class-wise F1 score. Additional gains are achieved by introducing regularization terms that enhance the model’s discriminative capacity, resulting in a further class-wise increase of 1.88% in AUC and 4.58% in F1 score. Regarding LADM specifically, the results in Table 8 demonstrate that using fixed, well-designed class-wise queries is generally more effective than learnable queries across most evaluation metrics.

To further analyze model behavior, we visualize the latent feature distributions of the test set using t-SNE under different architectural and training configurations. As shown in Figure 5, incorporating LADM for extracting single-class features, along with a predefined ETF classifier to regulate feature distribution across clients, enables the model to focus on semantic content rather than irrelevant factors such as the number of labels per sample. Furthermore, the addition of regularization terms during training leads to more compact and semantically coherent clusters, while also reducing the similarity among class-wise average prototypes. As shown in Figure 6, the pairwise cosine similarity between class-wise average features decreases with the inclusion of LADM and the ETF classifier, and is further reduced by the added regularization terms, indicating enhanced inter-class separability and stronger discriminative capability.

| ETF Clf | LADM | \mathcal{L}_{Neg} | \mathcal{L}_{Pos} | macro-AUC | macro-F1 | AUC | F1 |
|---------|------|----------------------------|----------------------------|--------------|--------------|--------------|--------------|
| | | | | 82.46 | 40.65 | 81.83 | 41.24 |
| ✓ | ✓ | | | 85.84 | 44.64 | 85.10 | 45.45 |
| ✓ | ✓ | ✓ | | 87.72 | 48.22 | 86.16 | 48.93 |
| ✓ | ✓ | | ✓ | 86.78 | 44.46 | 86.08 | 45.28 |
| ✓ | ✓ | ✓ | ✓ | 87.72 | 49.22 | 87.13 | 49.60 |

Table 7: Ablation study of the proposed method on the multi-label CIFAR10 dataset. β is set to 0.5 and γ is set to 0.5.

Experiments (additional)

To complement the results reported in the main manuscript and further validate the reproducibility of our method, we present additional experiments on the multi-label CIFAR-10

| query type | query init | macro-AUC | macro-F1 | AUC | F1 |
|------------|------------|--------------|--------------|--------------|--------------|
| learnable | random | 84.15 | 38.10 | 83.70 | 39.30 |
| learnable | ETF | 86.26 | 43.61 | 85.41 | 43.87 |
| fixed | ETF | 85.84 | 44.64 | 85.10 | 45.45 |

Table 8: Ablation study of the class-wise feature extraction block - LADM on the multi-label CIFAR10 dataset.

dataset (Krizhevsky et al., 2009). These experiments were repeated three times with different random seeds to evaluate the stability and effectiveness of the proposed approach. The mean and standard deviation of the results are reported in Table 9. As shown in the table, the proposed method demonstrates stable performance across multiple runs and consistently outperforms competing approaches.

Dataset

In this section, we introduce the datasets used in our experiments. To evaluate both the effectiveness and real-world applicability of the proposed method, we conduct experiments on datasets from general computer vision (CV) as well as medical imaging domains. Specifically, we use CIFAR-10 (Krizhevsky et al., 2009) and PASCAL VOC (Everingham et al., 2010) as general CV datasets, and DermaMNIST (Yang et al., 2023a) and ChestX-ray14 (Wang et al., 2017) as medical datasets. We simulate the FL system with 10 clients. To model non-IID data distributions, the data is partitioned using a Dirichlet distribution, with the concentration parameter β controlling the degree of heterogeneity. To further simulate missing-class scenarios, we constrain the number of classes available to each client using the class-presenting ratio γ , which specifies the proportion of total classes present locally. Dataset-specific settings are detailed below.

CIFAR-10 (Krizhevsky et al., 2009) is a widely used benchmark in CV. It comprises 10 classes: *airplane*, *automobile*, *bird*, *cat*, *deer*, *dog*, *frog*, *horse*, *ship*, and *truck*. To adapt CIFAR-10 for multi-label classification, following Li et al. (2023a), we create composite samples by combining multiple original images into a single image, with their corresponding labels forming a multi-label ground truth. Specifically, we retain a portion of the original single-label images and augment the dataset by creating an equal number of synthetic samples for each possible pairwise class combination. These composites are constructed by randomly selecting two images from different classes and combining them into one. We evaluate our method on the multi-label CIFAR-10 dataset under two FL configurations, using $\beta = 0.5$, $\gamma = 0.5$ and $\beta = 0.1$, $\gamma = 0.5$. Figure 8 illustrates the corresponding class-wise data distribution across clients.

DermaMNIST (Yang et al., 2023a) is a skin lesion classification dataset. It consists of 7 diagnostic categories: *actinic keratoses*, *basal cell carcinoma*, *benign keratosis-like lesions*, *dermatofibroma*, *melanocytic nevi*, *melanoma*, and *vascular lesions*. To adapt DermaMNIST for multi-label classification, we apply a strategy similar to the one used for multi-label CIFAR-10. Given the long-tailed nature of the original dataset,

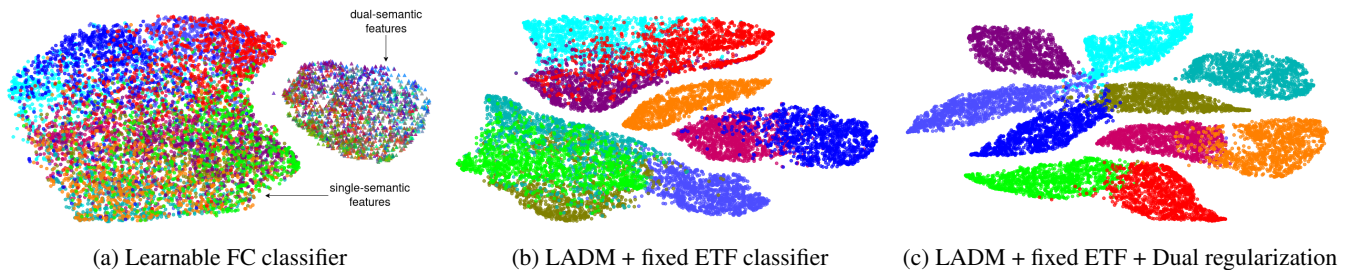


Figure 5: t-SNE visualisation of test data feature embeddings on the multi-label CIFAR10 experiment with $\beta = 0.5, \gamma = 0.5$. Each colour represents a class. Observing from subfigure (a), without feature disentanglement (LADM), the model appears to rely on undesired information, such as the number of labels per sample, for clustering.

| | $\beta = 0.5, \gamma = 0.5$ | | | |
|-------------------------------------|-----------------------------|-------------------------|-------------------------|-------------------------|
| | macro-AUC | macro-F1 | AUC | F1 |
| Centralized (Upperbound) | 92.20 \pm 0.36 | 61.30 \pm 0.94 | 90.04 \pm 0.65 | 62.02 \pm 0.62 |
| FedAvg (McMahan et al., 2017) | 82.29 \pm 0.46 | 39.47 \pm 1.59 | 81.48 \pm 0.78 | 40.26 \pm 1.09 |
| FedCurv (Shoham et al., 2019) | 82.53 \pm 0.30 | 39.96 \pm 1.28 | 82.10 \pm 0.29 | 40.34 \pm 1.04 |
| FedProx (Li et al., 2020) | 82.45 \pm 0.34 | 39.22 \pm 0.74 | 81.77 \pm 0.48 | 39.66 \pm 0.53 |
| SCAFFOLD (Karimireddy et al., 2020) | 82.51 \pm 0.44 | 39.98 \pm 1.41 | 82.08 \pm 0.53 | 40.26 \pm 1.26 |
| SphereFed (Dong et al., 2022) | <u>83.63</u> \pm 1.50 | 42.58 \pm 3.20 | <u>83.50</u> \pm 1.87 | 43.18 \pm 2.34 |
| FedLGT (Liu et al., 2024) | 83.52 \pm 0.68 | <u>43.60</u> \pm 1.68 | 83.36 \pm 0.71 | <u>44.03</u> \pm 1.71 |
| FedNAlign-ML (ours) | 87.55 \pm 0.31 | 49.17 \pm 1.65 | 87.00 \pm 0.31 | 49.61 \pm 1.64 |

Table 9: Comparisons on the multi-label CIFAR-10 dataset (Krizhevsky et al., 2009). Non-IID data distributions across clients are simulated using the Dirichlet concentration parameter (β) and the class-missing ratio (γ).

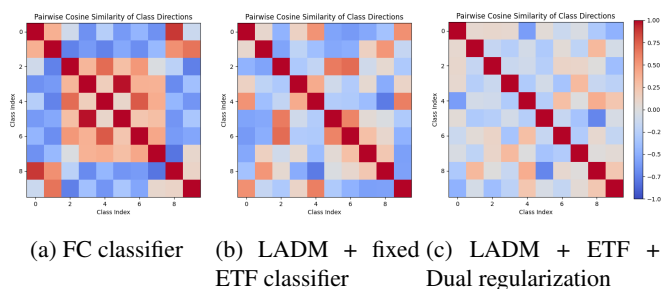


Figure 6: Pair-wise cosine similarity between test data class-wise average feature prototypes on the multi-label CIFAR10 dataset.

we preserve its inherent distribution by retaining all single-label samples. Then, we augment the dataset with an equal number of synthetic samples for each possible pairwise label combination. Figure 7 shows examples of the resulting composite multi-label inputs. The resulting dataset comprises the complete set of original samples along with the newly generated multi-label samples. We evaluate our method on this multi-label DermaMNIST dataset under two FL configurations: $\beta = 0.5, \gamma = 0.71$ and $\beta = 0.1, \gamma = 0.71$. The corresponding class-wise data distributions across clients are illustrated in Figure 9.

PASCAL VOC 2012 (VOC) (Everingham et al., 2010) is a widely used benchmark dataset in CV. It consists of approximately 11,500 images, each annotated with one or more object categories selected from a predefined set of 20 classes. These

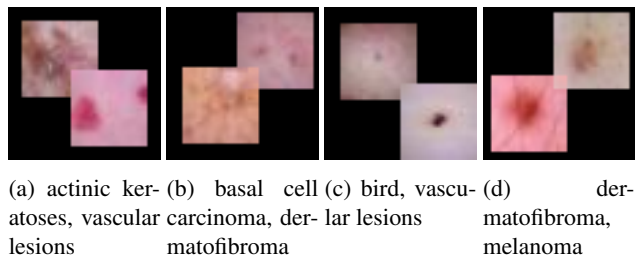


Figure 7: Examples from the multi-label DermaMNIST dataset. Each subfigure displays a composite image along with its corresponding set of labels.

object categories are: *aeroplane, bicycle, bird, boat, bottle, bus, car, cat, chair, cow, dining table, dog, horse, motorbike, person, potted plant, sheep, sofa, train, and TV monitor*. This dataset poses a challenging multi-label classification problem due to the presence of class imbalance, intra-class variability, and frequent inter-class co-occurrence. For example, the *person* category often co-occurs with many other object classes. Under a label-skewed FL setting, the non-IID distribution of data and inconsistencies in class co-occurrence patterns across clients further exacerbate the learning difficulty. We evaluate our method on VOC under two FL configurations, using $\beta = 0.05, \gamma = 0.5$ and $\beta = 0.01, \gamma = 0.5$. Figure 10 illustrates the resulting class-wise data distribution across clients.

ChestX-ray14 (Wang et al., 2017) is a large-scale medical imaging dataset commonly used for automated thoracic disease classification. It consists of 112,120 frontal-view chest

X-ray images collected from 30,805 unique patients. Each image is annotated with one or more disease labels, making the dataset naturally suitable for multi-label classification tasks. These labels were extracted from corresponding radiology reports using natural language processing techniques. The dataset includes 14 disease categories: *Atelectasis*, *Cardiomegaly*, *Consolidation*, *Edema*, *Effusion*, *Emphysema*, *Fibrosis*, *Hernia*, *Infiltration*, *Mass*, *Nodule*, *Pleural Thickening*, *Pneumonia*, and *Pneumothorax*. In addition, a *No Finding* label is used to indicate negative samples in which none of the 14 diseases are present. Due to its scale, real-world variability, and label noise, ChestX-ray14 provides a challenging benchmark for developing and evaluating deep learning models in medical image analysis, particularly in multi-label, imbalanced scenarios. We conduct experiments under two label-skewed FL settings on this dataset, using configurations of $\beta = 0.5, \gamma = 0.5$ and $\beta = 0.1, \gamma = 0.5$. Since a significant portion of the dataset is “No Finding” samples, we distribute these evenly across all clients in both settings. This setup mimics realistic clinical scenarios where healthy cases are common, while disease cases are relatively rare and unequally distributed across institutions. Figure 11 shows the class-wise data distribution across clients.



Figure 8: Distribution of data across local clients used in the experiments on the CIFAR-10 dataset (Krizhevsky et al., 2009).

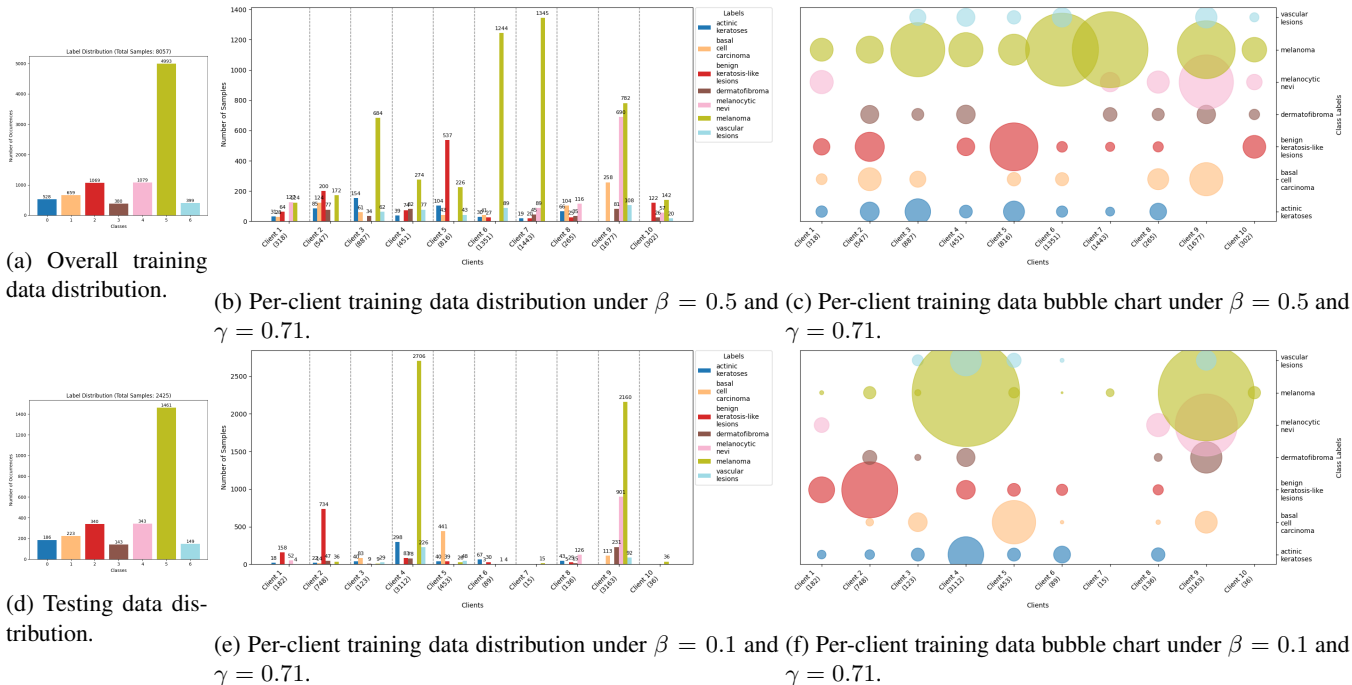


Figure 9: Distribution of data across local clients used in the experiments on the DermaMNIST dataset (Yang et al., 2023a).



Figure 10: Distribution of data across local clients used in the experiments on the VOC dataset (Everingham et al., 2010).

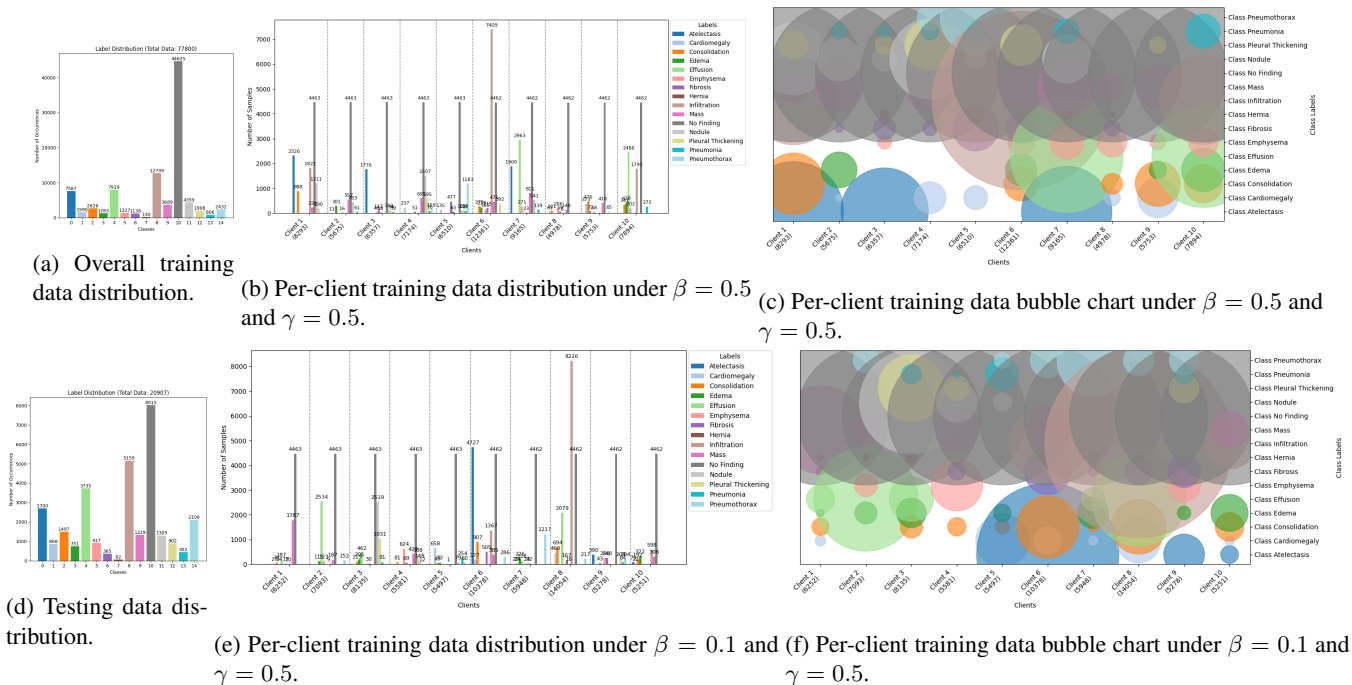


Figure 11: Distribution of data across local clients used in the experiments on the ChestX-ray14 dataset (Wang et al., 2017).